ELSEVIER

Journal of Power Sources 105 (2002) 228–238

JOURNAL OF POWER SOURCES

www.elsevier.com/locate/jpowsour

On the width of the electrochemically active region in mixed conducting solid oxide fuel cell cathodes

J. Fleig*

Max-Planck Institute for Solid State Research, Heisenbergstr. 1, 70569 Stuttgart, Germany

Abstract

The width of the electrochemically active zone in a mixed conducting solid oxide fuel cell (SOFC) cathode, i.e. the spatial extension of the three-phase-boundary (3PB) region is numerically calculated for the case when oxide ion transport through the electrode bulk determines the reaction rate of the cathodic oxygen reduction reaction. The current density distribution in the cathode exhibits a sharp maximum at the 3PB and a major fraction of the total current flows in narrow zones with a width of a few percent of the electrode particle size (e.g. in the case of 1.6 μm particle size: approximately 2/3 of the current flows in a zone with a width of 60 nm). Hence, the corresponding polarisation resistance is almost inversely proportional to the 3PB length. In a wide parameter range an increasing ionic conductivity of the mixed conductor does not broaden the electrochemically active region. A formula is presented which allows an estimate of the polarisation resistance of a mixed conducting electrode if ionic transport through the electrode bulk is rate limiting.

Keywords: Three-phase-boundary; Solid oxide fuel cells; Electrode polarisation; Mixed conductors; Cathodes

1. Introduction

The electrochemical performance of a solid oxide fuel cell (SOFC) strongly depends on the kinetics of the cathodic oxygen incorporation reaction. Numerous studies have been performed (e.g. on perovskites [1–28], platinum [29–33], gold [33,34] and silver electrodes [35,36]) to investigate the electrochemical mechanisms of this cathodic reaction but for none of these materials has a final agreement with respect to the rate-determining steps been achieved. Frequently the experimental results are discussed in terms of the following two reaction paths (see e.g. [4,6,10,11,14,23,28,35–39]): (i) the *surface path* includes adsorption of oxygen on the electrode surface, diffusion of a (probably dissociated and partly ionised) oxygen species along the surface towards the three-phase-boundary (3PB), complete ionisation, and an ionic transfer step into the electrolyte (Fig. 1a); (ii) the *bulk path* consists of oxygen dissolution in the electrode, oxygen transport through the electrode, ionisation step(s), and the transfer of the ion into the electrolyte. In the case of oxide cathodes (often perovskites) the oxygen incorporation into the electrode material includes the ionisation step (Fig. 1b) and hence the transport in the bulk is an ionic transport requiring a certain ionic conductivity. In doped $LaMnO_3$, which is the most widely used SOFC-cathode material, the ionic conductivity is rather low and it is usually assumed that the reaction via the surface path dominates the current although with certain electrode geometries or under high overvoltages significant oxide ion transport through doped $LaMnO_3$ cannot be excluded [4,6,11,16,28]. However, in mixed ionic and electronic conductors (MIECs) with considerable ionic conductivity the bulk path can be expected to be "open", thus lowering the polarisation resistance. This supposition has triggered many investigations on transport properties of MIECs and on their potential application as SOFC-cathodes.

In the case of a dominating surface path the electrochemically active, i.e. current-carrying region is probably restricted to a very narrow region around the 3PB. In MIECs, however, it is assumed that the active zone is broadened into the MIEC/electrolyte interface (often referred to as a spatial extension of the 3PB-region), and this extension is considered to become larger with increasing ionic conductivity [2,4,10,28]. Calculations have in the past been performed for the case that the kinetics of the oxygen exchange reaction at a porous MIEC-cathode considerably influence the polarisation resistance [25], yielding interesting information on the electrochemically active thickness of a mixed conducting cathode. However, since these simulations were one-dimensional and considered the MIEC as a continuum they only have a limited validity range. An equivalent circuit model taking into account both the surface and the bulk path

* Tel.: +49-711-689-1770; fax: +49-711-689-1722.
E-mail address: fleig@chemix.mpi-stuttgart.mpg.de (J. Fleig).

0378-7753/02/$ – see front matter
PII: S0378-7753(01)00944-2

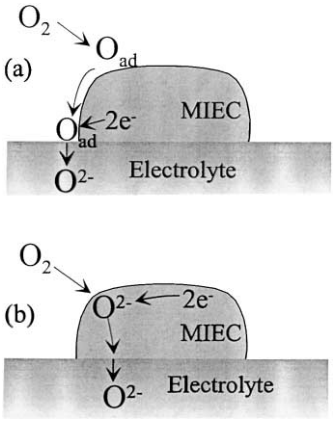

Fig. 1. Sketches of the surface path (a) and the bulk path (b) commonly used to discuss electrode kinetics on SOFC-cathodes. MIEC means mixed ionic and electronic conductor.

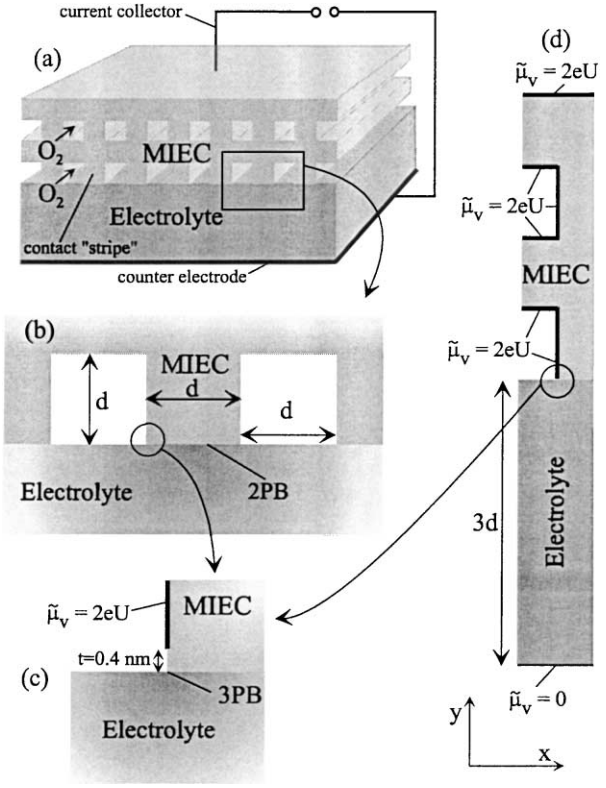

Fig. 2. (a) Model system considered in the finite element study presented; (b) magnification of a cross-section; (c) magnification of the 3PB-region indicating the region, t, where oxygen incorporation is prohibited; (d) basic element used to perform the calculations and boundary conditions with respect to $\tilde{\mu}_V$.

[40] is again based on a one-dimensional treatment of the current flow. Further one-dimensional studies present current–voltage characteristics for numerous kinetic situations [38,39], but an exact calculation of the multi-dimensional current distribution within the cathode particles has not been performed yet.

Particularly for the case of a predominant bulk path with transport through the electrode being the rate-determining step a rigorous study of the relation between the width of the electrochemically active zone/polarisation resistance on the one hand, and the ionic conductivity/electrode geometry on the other hand is still missing. It is, for example, unclear whether or not the electrochemically active zone really broadens if the ionic conductivity of the electrode is enhanced and it is also not evident how the polarisation resistance depends on the 3PB length and on the area of the MIEC/electrolyte interface.

In this contribution numerical finite element calculations are presented which deal with the effect of the ionic conductivity and the electrode geometry on the current distribution in a MIEC-cathode. In particular the current density distribution across the two-phase-boundary (2PB) between the MIEC and the electrolyte and hence the width of the electrochemically active zone is calculated for the case of a cathodic reaction with a predominant bulk path and transport of oxide ions in the cathode being the rate-determining step. It is discussed how this width and the polarisation resistance depend on the particle size and the ionic conductivity of the MIEC and it is estimated how large the ionic conductivity has to be in order to achieve a satisfactory polarisation resistance for an SOFC-cathode.

2. Model system and theoretical considerations

As discussed above (cf. Fig. 1) there are different possible reaction paths with respect to the electrochemical incorporation of oxygen into the SOFC electrolyte. The reaction rates of these parallel reaction paths depend on several parameters such as temperature, partial pressure, voltage and materials properties and under different experimental conditions different elementary steps of the oxygen reduction reaction can determine the overall reaction rate. The situation complicates even more if inhomogeneous material parameters, lead to spatially varying kinetic situations. A theoretical simulation of SOFC-cathodes requires a considerable reduction of their complexity and hence several geometrical and electrochemical assumptions. In this contribution the model geometry shown in Fig. 2 has been used to investigate the current density distribution in a mixed conducting electrode. It is assumed that the bulk path (cf. Fig. 1b) can be described by the consecutive steps: (i) dissociative adsorption of oxygen followed by ionisation and incorporation of oxide ions into the MIEC; (ii) ionic transport in the MIEC towards the MIEC/electrolyte interface; and (iii) ion transfer across this interface. It is further assumed that only this bulk path contributes to the overall current and that all reaction steps beside the transport of ions in the MIEC are very fast and do not influence the electrochemical performance. In other words, the transport of oxide ions in the MIEC is assumed to be the rate-determining step of the electrochemical reaction at the cathode. Accordingly, the oxygen exchange

reaction at the free surfaces (fs) of the cathodes (bold, black lines in Fig. 2d)

$$\tfrac{1}{2}O_2 + V_O^{\bullet\bullet}\,(\mathrm{MIEC}) \rightleftarrows O_O^x\,(\mathrm{MIEC}) + 2h^{\bullet}\,(\mathrm{MIEC}) \quad (1)$$

is in quasi-equilibrium and the electrochemical potential of the ionic charge carriers (vacancies) $\tilde{\mu}_V$ is continuous across the 2PB. Only the case of a hole-conducting MIEC is discussed but all considerations are equally valid for an electron-conducting MIEC.

The calculations were restricted to the dc case in which the hole current is blocked at the 2PB. This means that at the 2PB the electronic current density perpendicular to the interface vanishes and that the ionic current in the MIEC corresponds to the total current in the sample. The electronic conductivity in the MIEC is assumed to be large enough that only a negligible gradient of the electrochemical potential of the holes $\tilde{\mu}_h\,(\mathrm{MIEC})$ is necessary to enable the hole current to flow from the fs of the MIEC (where holes are created, Eq. (1)) to any current collector. In other words

$$\nabla\tilde{\mu}_h\,(\mathrm{MIEC}) \approx 0 \quad (2)$$

is assumed and it is as if the holes generated by the incorporation reaction are removed from the surface of the MIEC directly by a virtual current collector covering the entire surface. Hence, the electronic conductivity as well as the position of the current collector do not play any role and we only consider the ionic current density in the model sample.

The situation corresponds to the case of a Hebb–Wagner polarisation [41] with the fs being reversible for ionic and electronic charge carriers while the 2PB is reversible for ions and blocking for electrons/holes. It is worth mentioning that in a MIEC with high hole concentration, c_h, compared to its vacancy concentration, c_V, the electrical field is negligible in the dc case. In such a case the ionic dc current in the MIEC is mainly due to diffusion in a vacancy concentration gradient while in the electrolyte the field migration dominates. However, the calculations presented here are independent of the c_V/c_h ratio and also valid if the ionic current in the MIEC is field-driven.

Let us now mathematically define the problem to be solved. The total ionic current density in the model sample j_V is

$$j_V = -\left(\frac{\sigma_i}{2e}\right)\mathrm{grad}\,\tilde{\mu}_V \quad (3)$$

where σ_i represents the ionic conductivity of the MIEC or the electrolyte. In the dc case the divergence of the current density in both the MIEC and the electrolyte vanishes and if homogeneous conductivity values are assumed the equation

$$\mathrm{div}(\mathrm{grad}\,\tilde{\mu}_V) = 0 \quad (4)$$

has to be solved to obtain the ionic current density in the model system.

The boundary conditions with respect to the electrochemical potential of the vacancies $\tilde{\mu}_V$ are defined like this: applying a voltage U to the model sample means that the difference of the electrochemical potential of the holes between the entire MIEC and the reversible counter electrode (CE) $\Delta\tilde{\mu}_h$ reads

$$\Delta\tilde{\mu}_h = \tilde{\mu}_h\,(\mathrm{MIEC}) - \tilde{\mu}_h\,(\mathrm{CE}) = eU \quad (5)$$

Owing to the quasi-equilibrium of reaction (1) $\tilde{\mu}_V$ at the fs of the MIEC is given as

$$\tilde{\mu}_V\,(\mathrm{MIEC_{fs}}) = 2\tilde{\mu}_h\,(\mathrm{MIEC}) - \mu'_O \quad (6)$$

where μ'_O is the chemical potential of gaseous oxygen at the MIEC. (The electrochemical potential of the vacancies $\tilde{\mu}_V$ is defined for vacancies as building elements and hence includes O_O^x). The quasi-equilibrium of the reaction

$$\tfrac{1}{2}O_2 + V_O^{\bullet\bullet}\,(\mathrm{IC}) \rightleftarrows O_O^x\,(\mathrm{IC}) + 2h^{\bullet}\,(\mathrm{CE}) \quad (7)$$

at the non-polarisable interface between the CE and the ionic conductor (IC) yields

$$\tilde{\mu}_V\,(\mathrm{IC_{CE}}) = 2\tilde{\mu}_h\,(\mathrm{CE}) - \mu''_O \quad (8)$$

with $\tilde{\mu}_V\,(\mathrm{IC_{CE}})$ being the electrochemical potential of the vacancies in the IC at the CE. Assuming the same chemical potential of gaseous oxygen ($\mu''_O = \mu'_O$) at the CE and the MIEC, i.e. a uniform oxygen partial pressure, the applied voltage $U = \Delta\tilde{\mu}_h/e$ directly leads to

$$\Delta\tilde{\mu}_V = \tilde{\mu}_V\,(\mathrm{MIEC_{fs}}) - \tilde{\mu}_V\,(\mathrm{IC_{CE}}) = 2eU \quad (9)$$

Thus, the boundary conditions used to solve Eq. (2) are

$$\tilde{\mu}_V\,(\mathrm{MIEC_{fs}}) = 2eU \quad (10)$$

and

$$\tilde{\mu}_V\,(\mathrm{IC_{CE}}) = 0 \quad (11)$$

see also Fig. 2d.

A further assumption with respect to the boundary conditions has been made: close to the 3PB the differentiation between bulk and surface path (Fig. 1) is no longer useful. If, for example, the vacancy in the MIEC enabling the oxygen incorporation (Eq. (1)) is directly at the MIEC/electrolyte interface no further transport through the bulk is necessary to run the cathodic reaction and such a situation pertains to the surface path (Fig. 1). It has therefore been assumed that the free surface being electrochemically active with respect to the bulk path ends a certain distance, t, from the 3PB. In most calculations a value of 0.4 nm, which is close to the lattice constant of many cubic perovskites, was used. The dependence of the quantitative results on this width, t, is discussed in Section 3 but all essential conclusions are, in the t-range considered here (0.4–8 nm), independent of the width of this inactive zone. It has to be emphasised that the surface path may play an important role also in mixed conducting cathodes (cf. [40]). However, in this paper we concentrate on the effects of the bulk path with bulk transport being rate-determining and, for the sake of clarity, do not consider the additional current via the surface path.

Since we restrict the consideration to small voltages ($U = 20$ mV) the influence of any vacancy gradient on the local ionic conductivity $\sigma_{i,MIEC}$ of the MIEC can be neglected. Grain boundaries as possible fast conductance paths are not taken into account and hence homogeneous $\sigma_{i,MIEC}$ values (10^{-7} to 10^{-1} S/cm) are assumed. The electrolyte is regarded to be a pure IC with conductivity $\sigma_{IC} = 10^{-1}$ S/cm. The contact width (d) of the model geometry (Fig. 2) is varied from 200 nm to 4 μm. As long as the electrolyte is thick compared to the size of the electrochemically active regions of the 2PB the current distribution in the MIEC can be expected to be independent of the electrolyte thickness [42]. Hence, an electrolyte thickness of three times the contact width, i.e. 600 nm–12 μm has been used. Because of the symmetrical set-up it is sufficient to solve Eq. (4) in two dimensions for the basic element shown in Fig. 2d. The finite element software package FLUXEXPERT (SIMULOG, France) was applied to numerically calculate $\tilde{\mu}_V$, grad $\tilde{\mu}_V$ and the integral of the current density.

3. Results and discussion

3.1. Width of the electrochemically active zone

It has already been discussed that in mixed conducting electrodes the oxygen reduction reaction is not restricted to the corresponding 3PB line. The region where oxygen is reduced is extended onto the free surface of the MIEC and the region where oxide ions are incorporated into the electrolyte is extended into the 2PB between the MIEC and the electrolyte. These two effects are correlated and we restrict the discussion to the width of the electrochemically active zone at the 2PB. Since the current density does not vanish across the 2PB there is some arbitrariness in the definition of this width. In this work the two following definitions are used: (i) the *integral width* ($w_{2/3}$) corresponds to the width of the two stripes of the 2PB region which carry 2/3 of the total current; (ii) the *decay width* (w_λ) is defined as the distance from the 3PB at which the current density amounts to 20% of its maximum value at the 3PB.

Fig. 3 shows a cross-section of $\tilde{\mu}_V$ equipotential lines for $\sigma_{i,MIEC} = 10^{-7}$ S/cm and $d = 1.6$ μm. Obviously the gradient of the electrochemical potential of the vacancies is largest close to the 3PB indicating that a considerable amount of the oxide ion transport through the cathode bulk is concentrated close to the 3PB. Such a distribution has qualitatively already been predicted in [4]. Almost identical distributions result for all $\sigma_{i,MIEC}$ values $\leq 10^{-2}\sigma_{IC}$. The current density distribution across the 2PB of one contact "stripe" (cf. Fig. 2) is given in Fig. 4 and confirms that j_V is strongly enhanced close to the 3PB. The current density at the 3PB is almost independent of the contact widths (d) (Fig. 4b) while its value in the centre of the 2PB becomes smaller the larger is d (Fig. 4c). Please note that the profiles in Fig. 4c are logarithmic plots versus normalised distances.

Fig. 5 shows the relation between the integrated current density $\int_{3PB}^{x'} j\,dx'$ and the distance x from the 3PB for $\sigma_{i,MIEC} = 10^{-7}$ S/cm. Two narrow regions, each of them exhibiting a width of a few percent of the contact width, carry 2/3 of the total current. To give an example: in the case of 1.6 μm contact stripes an integral width $w_{2/3}$ of ≈60 nm results. Further widths are summarised in Table 1. The integral width ($w_{2/3}$) depends somewhat on the electrode

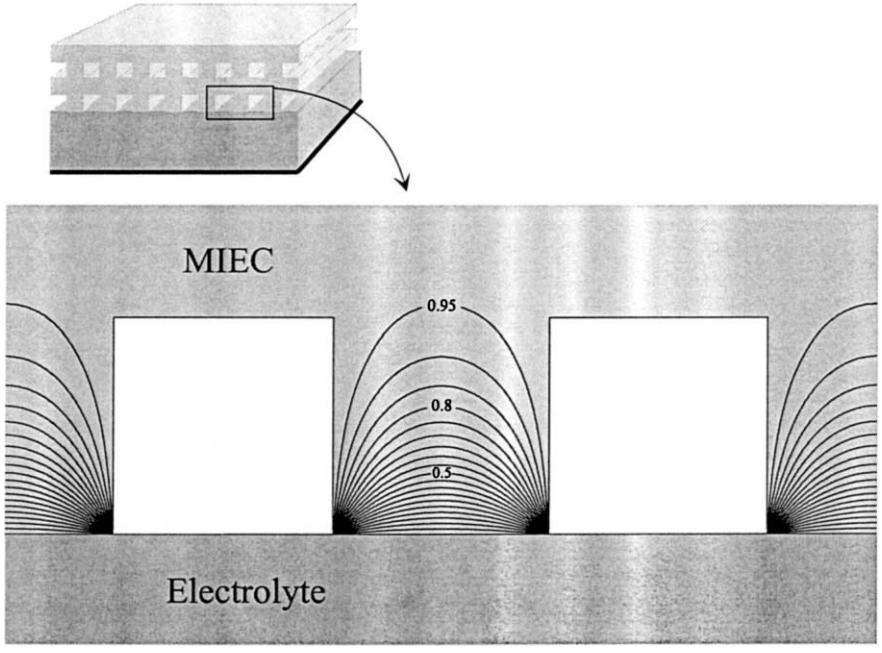

Fig. 3. Equipotential lines of $\tilde{\mu}_V$ in a cross-section for $\sigma_{i,MIEC} = 10^{-7}$ S/cm, $\sigma_{IC} = 10^{-1}$ S/cm, $d = 1.6$ μm, $t = 4$ nm, and $U = 20$ mV. The labels indicate the fraction of the total potential difference $2eU$.

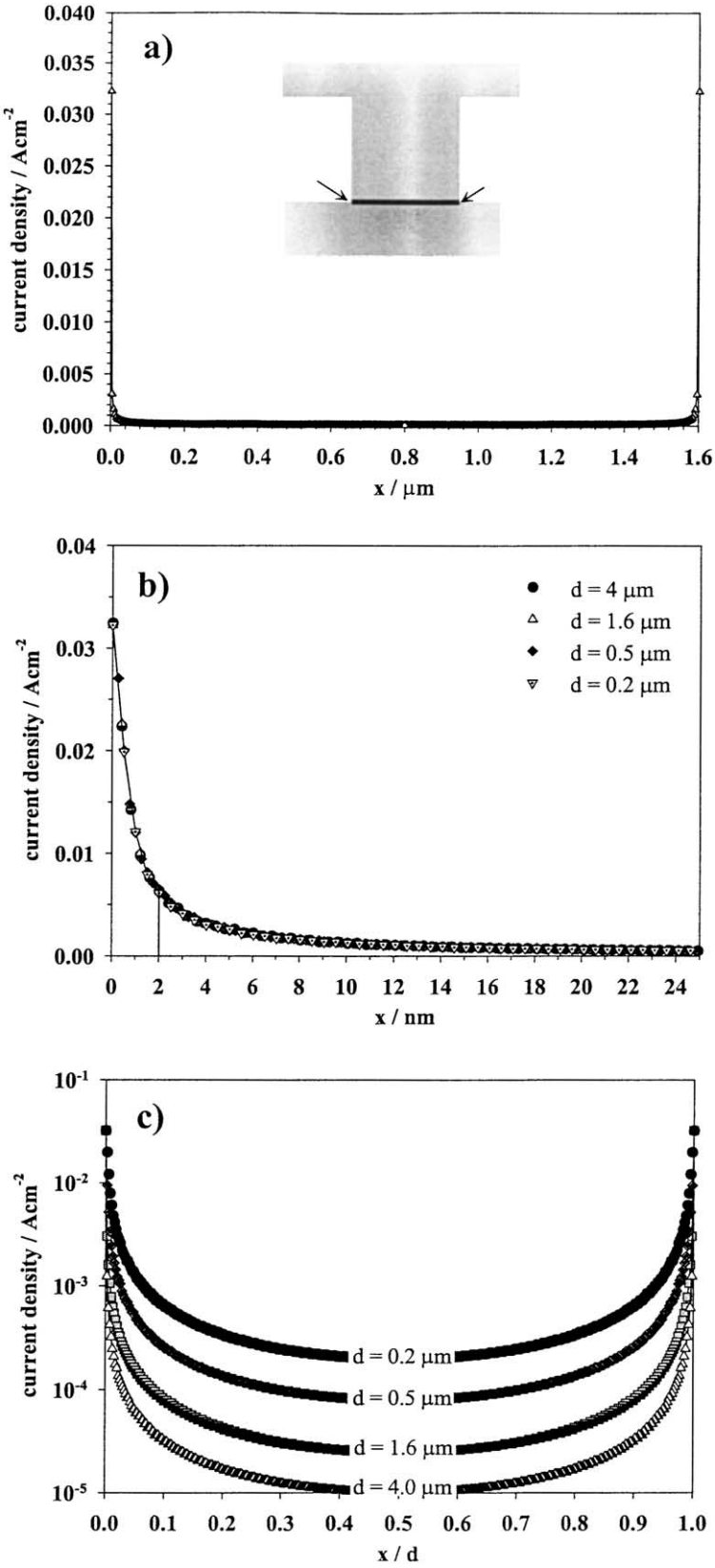

Fig. 4. Current density distributions across the 2PB for one contact stripe with $\sigma_{i,MIEC} = 10^{-7}$ S/cm, $\sigma_{IC} = 10^{-1}$ S/cm, $t = 0.4$ nm, and $U = 20$ mV. (a) Linear plot for $d = 1.6$ μm, the sketch indicates the location of the investigated line; (b) magnification of the region close to the three-phase-boundary for four different d values demonstrating that the decay length w_λ (solid line) does not depend on d; (c) logarithmic plot for four different stripe widths, the x-axis is normalised with respect to the stripe width.

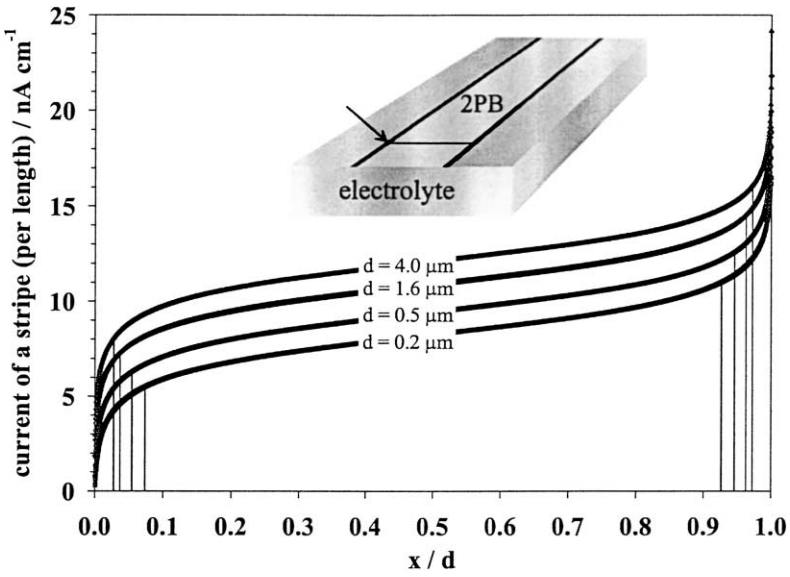

Fig. 5. Current of one contact stripe (normalised to the stripe length) integrated up to a certain fraction, x, of the stripe width for $\sigma_{i,MIEC} = 10^{-7}$ S/cm, $\sigma_{IC} = 10^{-1}$ S/cm, $t = 0.4$ nm, and $U = 20$ mV. The vertical lines indicate the integral widths, $w_{2/3}$, at which 2/3 of the total current flowing in one-half of a stripe is reached. The sketch illustrates the current-carrying areas (black) of the two phase boundary (2PB) and the integration path (indicated by an arrow).

Table 1
Integral width $w_{2/3}$ of the electrochemically active zone normalised to the stripe width d for different t values

d (µm)	$w_{2/3}/d$ for $t = 0.4$ nm	$w_{2/3}/d$ for $t = 1.0$ nm	$w_{2/3}/d$ for $t = 3.2$ nm	$w_{2/3}/d$ for $t = 8$ nm
0.2	0.0735	0.0995	–	–
0.5	0.0545	0.0735	–	–
1.6	0.037	–	0.0735	0.0995
4.0	0.0275	0.037	0.0545	0.0735

geometry and increases with increasing t values (inactive free surface). However, in a wide parameter range (cf. Table 1) $w_{2/3}$ only amounts to a few percent of the contact stripe width.

The decay width w_λ for $\sigma_{i,MIEC} = 10^{-7}$ S/cm can be read from Fig. 4b and is almost identical for all contact stripes, namely ≈2 nm if an inactive free surface region width of $t = 0.4$ nm is assumed. However, w_λ depends strongly on this inactive region and in general $w_\lambda \approx 5t$ results, at least for the geometries investigated here.

One might intuitively assume that the active zone becomes broader if the ionic conductivity of the MIEC is enhanced (“spatial extension of the 3PB-region”). However, Fig. 6 illustrates that this is usually not the case: the shape of the current distribution and thus the current lines do not depend on the ionic conductivity of the MIEC as long as $\sigma_{i,MIEC}$ is considerably smaller than the electrolyte conductivity. As shown in Fig. 6b, the electrochemically active width of the 2PB is in a wide parameter range conductivity-independent. Even if $\sigma_{i,MIEC}$ is of the order of magnitude of σ_{IC} the current density distribution broadens only moderately and the current is still constricted close to the 3PB. The enhancement of the integral width $w_{2/3}$ for very high $\sigma_{i,MIEC}$ can be explained by the current constriction in the electrolyte close to the electrochemically active zone [43]: for high $\sigma_{i,MIEC}$ values the additional electrolyte resistance due to this current constriction becomes important and the active zone is broadened in order to lower this current constriction resistance.

From these calculations we see that not only the surface path but also the bulk path with rate-determining ionic transport typically leads to narrow current-carrying zones close to the 3PB. This also means that a polarisation experiment in $^{18}O_2$ atmosphere with a subsequent SIMS-detection of the incorporated ^{18}O species [22] is excellent for monitoring the electrochemically active areas of an electrode but often cannot answer the question which path actually determines the current: not only the surface path but also the bulk path with transport as the rate-determining step should yield a U-shaped ^{18}O profile similar to the current density profiles shown in Fig. 4. However, the observation of an enhanced incorporation at the 3PB excludes that the incorporation reaction according to Eq. (1) or the transfer across the 2PB are rate-determining steps since in these cases rather homogeneous current density profiles can be expected (see also Section 3.3).

3.2. Geometry and conductivity dependence of the polarisation resistance

From a technological point of view it is important to know how the polarisation resistance depends on the geometry and the ionic conductivity of the cathode. From Fig. 5 it can be seen that the current per stripe does only slightly depend on the stripe width: an increase of the contact width by a factor

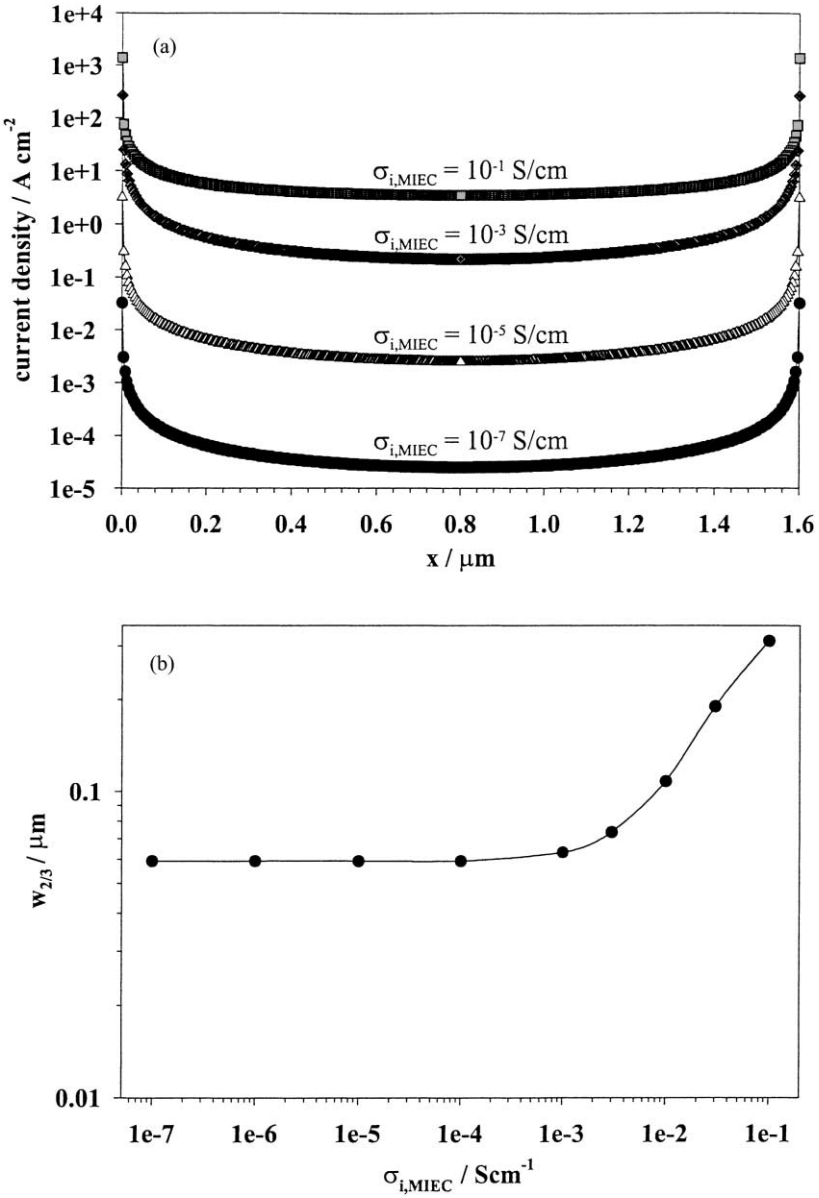

Fig. 6. (a) Logarithmic plot of the current density distribution across the 2PB of one contact stripe for different $\sigma_{i,MIEC}$, $d = 1.6$ μm, $\sigma_{IC} = 10^{-1}$ S/cm, $t = 0.4$ nm and $U = 20$ mV; (b) conductivity dependence of the integral width ($w_{2/3}$) of the electrochemically active zone for $d = 1.6$ μm, $\sigma_{IC} = 10^{-1}$ S/cm, and $t = 0.4$ nm.

of 20 leads to an increase of the current per stripe by less than a factor of 2. Considering that most of the current flows close to the 3PB and that the 3PB length of a stripe does not depend on its width, this result is not surprising. On the other hand, the number of contact stripes per area and thus the number of 3PBs per area is proportional to $1/d$ and the total current per area (I/A) increases strongly with decreasing contact width (Fig. 7a). Fig. 7a also shows that the current resulting for a dense MIEC-cathode with thickness d is much smaller than the current obtained for the porous structure considered here, which again demonstrates the importance of ''edge effects'' (incorporation close to the 3PB). The data can also be expressed in terms of a relation between the resistance and the 3PB length (Fig. 7b), leading to the result that the area-related polarisation resistance is almost inversely proportional to the 3PB length per area.

If other contact geometries are considered similar results can be expected as long as the cross-sections of the contact ''stripes'' or particles do not exhibit extreme aspect ratios. If, however, very thin and broad stripes are used the edge effects leading to the dominance of the 3PB-region are less important and most of the current flows in the broad centre of the contact. A current being almost proportional to the 2PB area rather than to the 3PB length can then be expected. Polarisation resistances of thin, dense Sr-doped $LaMnO_3$-microelectrodes with extreme aspect ratios have, for example, been reported to exhibit such an inverse proportionality to the contact area [16].

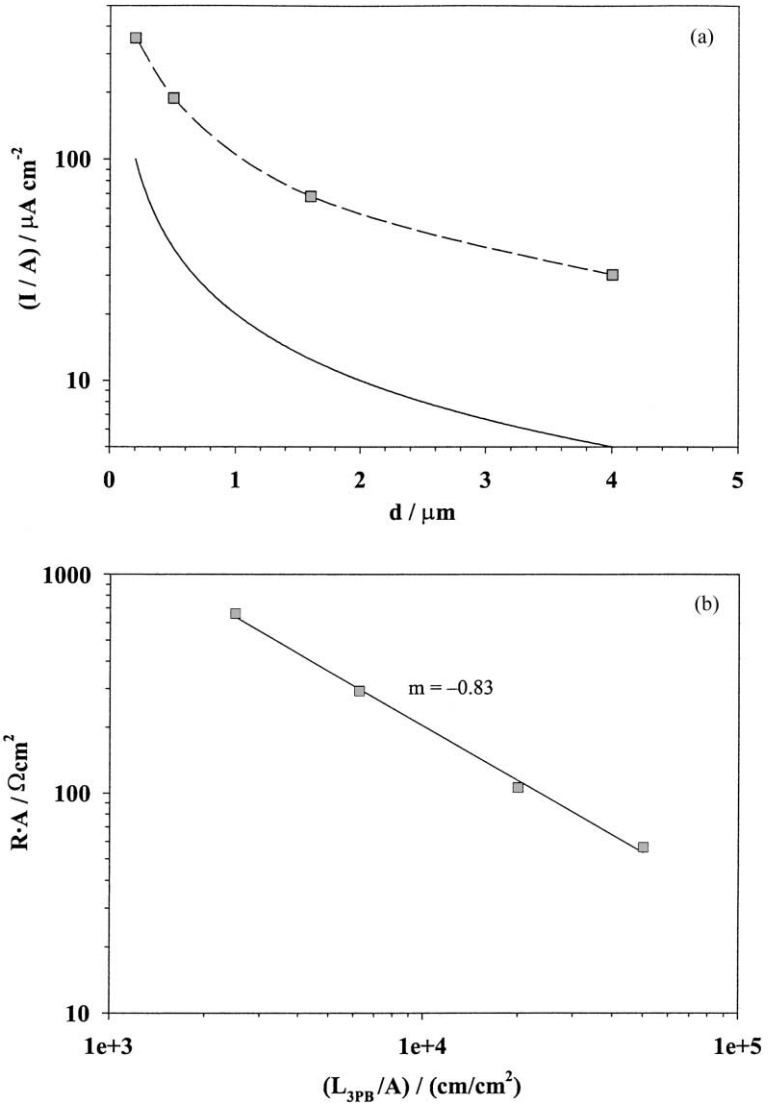

Fig. 7. (a) Total current per area for different stripe widths; $\sigma_{i,MIEC} = 10^{-7}$ S/cm, $\sigma_{IC} = 10^{-1}$ S/cm, $t = 0.4$ nm, and $U = 20$ mV. The solid line shows the current per area for the case that a dense MIEC-cathode with thickness d is used; (b) area-related resistance in dependence of the 3PB length per area for the same parameters. The slope of -0.83 indicates that the resistance is almost inversely proportional to the 3PB length.

The relation between polarisation resistance and ionic conductivity of the MIEC is presented in Fig. 8. For a broad range of conductivity values the total polarisation resistance is inversely proportional to $\sigma_{i,MIEC}$. Only if $\sigma_{i,MIEC}$ is of the order of σ_{IC} the resistance becomes rather independent of $\sigma_{i,MIEC}$. This is due to the fact that the current calculated from the numerically obtained current density distribution is not only limited by the electrode polarisation but also by the ohmic resistance of the thin electrolyte layer. For large $\sigma_{i,MIEC}$ values the latter part dominates.

3.3. Estimate of the transport resistance of geometrically realistic porous MIEC-cathodes

Real porous SOFC-cathodes exhibit a very complex electrochemical behaviour which is not only influenced by external parameters such as temperature, partial pressure, overvoltage or geometry but also depends on preparation conditions, thermal/chemical/electrical history, etc. (see e.g. [1–28]). Hence, an interpretation of the existing literature in terms of only one rate-determining step cannot be successful. Nevertheless it is worthwhile to estimate how a geometrically realistic MIEC-cathode electrochemically behaves if the bulk path dominates the oxygen reduction reaction and the ionic transport in the MIEC is the rate-determining step. This allows us, for example, to estimate which ionic conductivity is required in order to use a MIEC-cathode with predominant bulk path in SOFCs.

In a real electrode the MIEC-particles exhibit different sizes and shapes and constitute a complicated pattern of 3PB lines. However, since these particles usually do not have extreme aspect ratios the current close to the 3PB again dominates the total current and the considerations made for the model electrode in Fig. 2 are still valid. In particular the

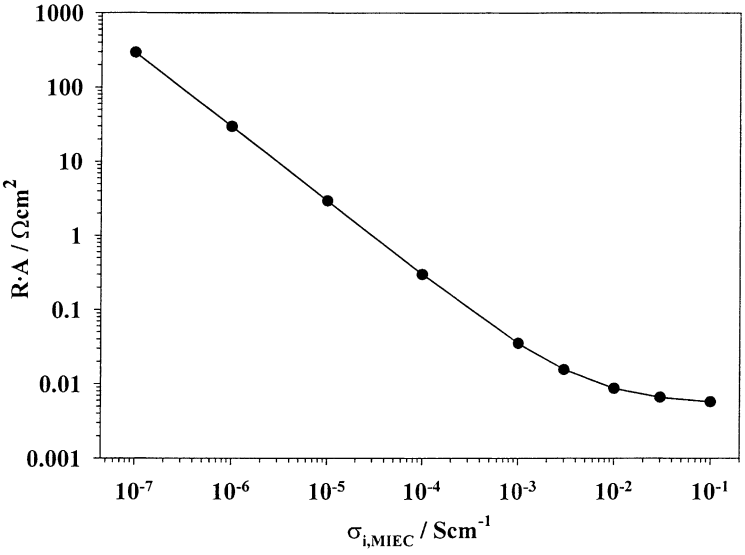

Fig. 8. Area-related resistance for $\sigma_{IC} = 10^{-1}$ S/cm, $d = 1.6$ μm and $t = 0.4$ nm as a function of the ionic conductivity of the MIEC. As long as $\sigma_{i,MIEC} \ll \sigma_{IC}$ the resistance is inversely proportional to $\sigma_{i,MIEC}$.

resistance per 3PB length density (Fig. 7b) can be expected to be independent of the exact shape of the particles. Hence, the area-related polarisation resistance of a real cathode $R_A = R \times A$ can be approximated by

$$R_A \approx R_{3PB} \frac{1}{L_{3PB}/A} \tag{12}$$

with R_{3PB} being an estimate of the resistance per 3PB length ($R \times L_{3PB}$) which we can obtain from the calculations presented. From Fig. 5 we see that the current per 3PB length I_{3PB} is approximately 10^{-8} A/cm for $\sigma_{i,MIEC} = 10^{-7}$ S/cm and a resistance per 3PB length ($R_{3PB} = U/I_{3PB}$) of $\approx$2 MΩ cm results. Since the current turned out to be proportional to $\sigma_{i,MIEC}$ (cf. Fig. 8) this can be generalised to

$$R_{3PB} \approx \frac{1}{5\sigma_{i,MIEC}} \tag{13}$$

The 3PB length per area can only roughly be estimated: let us assume an average particle size d'. In the case of cubic particles a 3PB length per particle $L_{3PB} = 4d'$ would result. However, real particles exhibit wavy or even fractal-like 3PB lines. Therefore, one could expect an enhanced 3PB length per particle. For a first approximation let us assume $L_{3PB} \approx 10d'$ and if 30% of the electrolyte surface is covered by such particles $L_{3PB}/A \approx 3/d'$ results. This means that, for example, for 0.6 μm particles a 3PB length of 5×10^4 cm/cm^2 can be calculated which corresponds to the value experimentally obtained in [3]. Hence, a polarisation resistance of

$$R_A \approx \frac{d'}{15\sigma_{i,MIEC}} \tag{14}$$

results if $\sigma_{i,MIEC} \ll \sigma_{IC}$ is assumed.

In real SOFCs a cathodic polarisation resistance of $\approx$0.15 Ω cm^2 can be regarded to be acceptable [14]. Using Eq. (14) we can estimate the ionic conductivity of the MIEC which is at least necessary to reach this value: for a particle size of 0.6 μm a value of $\approx 3 \times 10^{-5}$ S/cm, or in terms of a diffusion coefficient at 1100 K an oxygen self-diffusion coefficient of $D \approx 9 \times 10^{-11}$ cm^2/s, is sufficient. The ionic conductivity can be even lower if MIEC/electrolyte composite cathodes [44] with a three-dimensional mesh of 3PB lines and hence a considerably enhanced 3PB length per area are used. Moreover a cathodic overvoltage increases the oxygen vacancy concentration and thus the ionic conductivity of the MIEC which again lowers the resistance. In other words, already rather low ionic conductivities (<10^{-6} S/cm) could yield low cathodic resistances if no further kinetic hindrances play a role. For example, ionic conductivities obtained for cobaltites or ferrites [14,45–49] are, from the transport point of view, by far not necessary to achieve satisfactory cathodes and even the ionic conductivity of heavily Sr-doped $LaMnO_3$ is not so far from the desired value [48,50].

However, as already mentioned above this estimate is only true if (i) the bulk path dominates the reaction rate and (ii) transport in the MIEC is rate limiting. If, e.g. the oxygen incorporation reaction into the MIEC (Eq. (1)) is no longer in quasi-equilibrium and hence influences the polarisation resistance the situation changes completely. Various studies revealed that surface effects can strongly influence the polarisation resistance of MIEC-cathodes [14,25,26,51,52]. As an example, Fig. 9a shows the $\tilde{\mu}_V$ equipotential lines in the cathode if the oxygen exchange at the surface is rate limiting. A relatively uniform potential distribution results and the current density distribution at the 2PB (Fig. 9b) shows that the current is no longer restricted to the region close to the 3PB. The surface area of the MIEC could be expected to play a more important role than the 3PB length. In terms of the active zone a change from transport

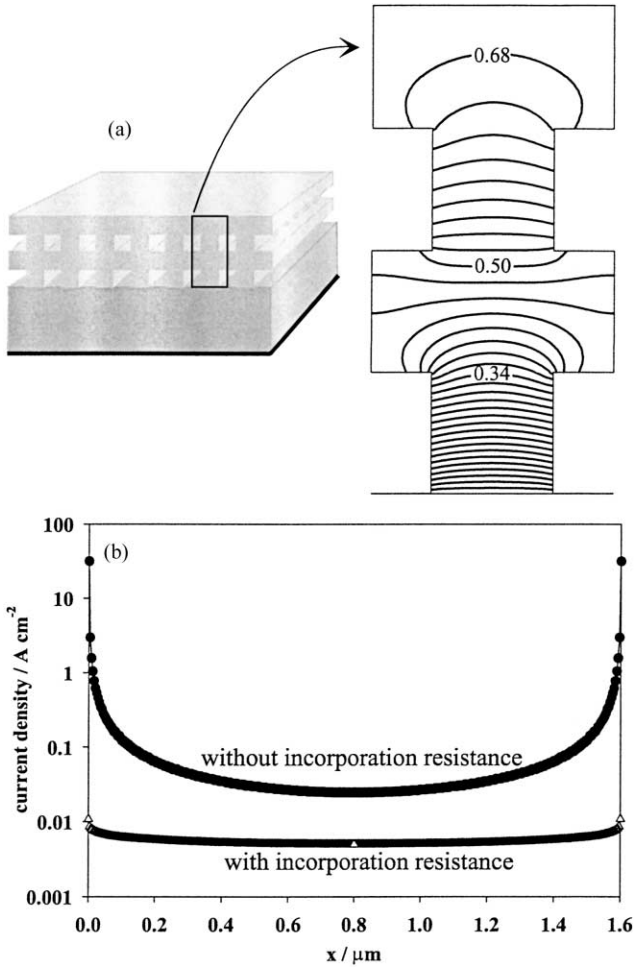

Fig. 9. (a) Equipotential lines of $\tilde{\mu}_V$ for $\sigma_{i,MIEC} = 10^{-4}$ S/cm, $\sigma_{IC} = 10^{-1}$ S/cm, $d = 1.6$ μm, $t = 0.4$ nm, $U = 20$ mV, and an area-related resistance due to the oxygen incorporation reaction into the MIEC of 16 W cm^2. The labels indicate the fraction of the total potential difference $2eU$; (b) current density distribution across the 2PB for $\sigma_{i,MIEC} = 10^{-4}$ S/cm, $\sigma_{IC} = 10^{-1}$ S/cm, $d = 1.6$ μm with (16 W cm^2) and without a resistance due to the oxygen incorporation reaction on the MIEC-surface.

limitation to oxygen incorporation limitation "activates" the entire 2PB, i.e. strongly broadens the 3PB-region. In contrast to the case shown in Fig. 3 the oxygen incorporation reaction into the MIEC is not limited to the "particles" (contact stripes) in contact with the electrolyte and since many "particle layers" are involved in the electrochemical reaction a continuum model of the porous electrode can be reasonable [25,53].

With respect to the applicability of MIECs as SOFC-cathodes one further conclusion can be drawn: SIMS-measurements on different MIECs revealed that an increasing ionic conductivity of the MIEC is usually accompanied by an increase of the oxygen exchange coefficient k [48]. However, in perovskites the increase of k is often less pronounced than the conductivity increase and surface processes can be expected to play a more important role in MIECs with comparably high ionic conductivity. Hence, in MIECs with high ionic conductivity the electrochemically active reaction zone is probably indeed broadened, but due to surface limitations and not because of the high ionic conductivity itself. This also means that in order to achieve the goal of a low-polarisable MIEC-cathode efforts to optimise the oxygen incorporation resistance (e.g. by surface treatment or by coverage with catalytic particles [23,54]) are required while very high ionic conductivities are not really necessary.

4. Conclusions

If the mechanism of the oxygen reduction reaction at a porous mixed conducting SOFC-cathode consists of oxygen incorporation into the cathode, transport of oxide ions to the 2PB and ion transfer into the electrolyte, and if the transport of the oxide ions in the cathode bulk is rate-determining, the following conclusions can be drawn.

- Within a distance of a few nanometers the ionic current density across the 2PB drops to 20% of its value at the 3PB. Within a narrow stripe of the 2PB region (typical width ≈3–6% of the particle size) 2/3 of the total ionic current flows. Hence, even for mixed conductors the current is strongly constricted to the 3PB-region if interface effects do not play any role.
- Increasing the ionic conductivity of the cathode does not broaden the active zone as long as the conductivity of the electrolyte is substantially higher than the ionic conductivity of the electrode.
- The polarisation resistance of mixed conducting porous SOFC-cathodes with transport limitation is almost inversely proportional to the 3PB length. Its area-related value R_A can roughly be estimated to be $R_A \approx d'/15\sigma_{i,MIEC}$ with d' and $\sigma_{i,MIEC}$ being the particle size and the ionic conductivity of the mixed conducting cathode. Therefore, from a transport point of view an ionic conductivity of $\sigma_{i,MIEC} = (1-5) \times 10^{-5}$ S/cm could already be sufficient to achieve a cathodic SOFC polarisation resistance of $0.15\,\Omega\,cm^2$. In composite cathodes even values $<10^{-6}$ S/cm might be possible.
- The situation completely changes if the oxygen incorporation reaction into the mixed conducting cathode becomes relevant. Then the effective 3PB-region broadens and the entire 2PB becomes electrochemically active.

References

[1] J. Mizusaki, H. Tagawa, K. Tsuneyoshi, A. Sawata, J. Electrochem. Soc. 138 (1991) 1867.
[2] J. Van Herle, A.J. McEvoy, K.R. Thampi, Electrochim. Acta 41 (1996) 1447.
[3] A. Mitterdorfer, L.J. Gauckler, Solid State Ionics 111 (1998) 185.
[4] E. Siebert, A. Hammouche, M. Kleitz, Electrochim. Acta 40 (1995) 1741.
[5] M.J.L. Ostergard, M. Mogensen, Electrochim. Acta 38 (1993) 2015.

[6] J. Mizusaki, T. Saito, H. Tagawa, J. Electrochem. Soc. 143 (1996) 3065.
[7] H.Y. Lee, W.S. Cho, S.M. Oh, H.-D. Wiemhöfer, W. Göpel, J. Electrochem. Soc. 142 (1995) 2659.
[8] H. Fukunaga, M. Ihara, K. Sakaki, K. Yamada, Solid State Ionics 86–88 (1996) 1179.
[9] H. Kamata, A. Hosaka, J. Mizusaki, H. Tagawa, Solid State Ionics 106 (1998) 237.
[10] A. Hammouche, E. Siebert, A. Hammou, M. Kleitz, A. Caneiro, J. Electrochem. Soc. 138 (1991) 1212.
[11] A. Endo, M. Ihara, H. Komiyama, K. Yamada, Solid State Ionics 86–88 (1996) 1191.
[12] M. Odgaard, E. Skou, Solid State Ionics 86–88 (1996) 1217.
[13] F.P.F. Berkel, F.H. van Heuveln, J.P.P. Huijsmans, Solid State Ionics 72 (1994) 240.
[14] B.C.H. Steele, Solid State Ionics 86–88 (1996) 1223.
[15] K. Sasaki, J.-P. Wurth, R. Gschwend, M. Gödickemeier, L.J. Gauckler, J. Electrochem. Soc. 143 (1996) 530.
[16] V. Brichzin, J. Fleig, H.-U. Habermeier, J. Maier, Electrochem. Solid State Lett. 3 (2000) 403.
[17] S. Wang, Y. Jiang, Y. Zhang, J. Yan, W. Li, J. Electrochem. Soc. 146 (1998) 1932.
[18] F.H. van Heuveln, H.J.M. Bouwmeester, F.P.F. van Berkel, J. Electrochem. Soc. 144 (1997) 126.
[19] F.H. van Heuveln, H.J.M. Bouwmeester, J. Electrochem. Soc. 144 (1997) 134.
[20] L.G.J. de Haart, R.A. Kuipers, K.J. de Vries, A.J. Burggraaf, J. Electrochem. Soc. 138 (1991) 1970.
[21] O. Yamamoto, Y. Takeda, Y. Tomida, M. Noda, Solid State Ionics 22 (1987) 241.
[22] T. Horita, K. Yamaji, M. Ishikawa, M. Sakai, H. Yokokawa, T. Kawada, T. Kato, J. Electrochem. Soc. 145 (1998) 3196.
[23] G.M. Christie, F.H. van Heuveln, F.P.F. van Berkel, in: F.W. Poulsen, N. Bonanos, S. Linderoth, M. Mogensen, B. Zachau-Christiansen (Eds.), Proceedings of the 17th Riso International Symposium on Material Science: High Temperature Electrochemistry: Ceramics and Metals, Riso National Laboratory, Roskilde, Denmark, 1996, p. 205.
[24] J. Divisek, L.G.J. De Haardt, P. Holtappels, T. Lennartz, W. Mallener, U. Stimming, K. Wippermann, J. Power Sources 49 (1994) 257.
[25] S.B. Adler, J.A. Lane, B.C.H. Steele, J. Electrochem. Soc. 143 (1996) 3554.
[26] S.B. Adler, Solid State Ionics 111 (1998) 125.
[27] M. Liu, Z. Wu, Solid State Ionics 107 (1998) 105.
[28] B. Gharbage, T. Pagnier, A. Hammou, J. Electrochem. Soc. 141 (1994) 2118.
[29] M.J. Verkerk, M.W.J. Hammink, A.J. Burggraaf, J. Electrochem. Soc. 130 (1983) 70.
[30] D.Y. Wang, A.S. Nowick, J. Electrochem. Soc. 126 (1979) 1155.
[31] E.J.L. Schouler, M. Kleitz, J. Electrochem. Soc. 134 (1987) 1045.
[32] J. Mizusaki, K. Amano, S. Yamauchi, K. Fueki, Solid State Ionics 22 (1987) 313.
[33] C. Schwandt, W. Weppner, J. Electrochem. Soc. 144 (1997) 3728.
[34] B.A. van Hassel, B.A. Boukamp, A.J. Burggraaf, Solid State Ionics 48 (1991) 155.
[35] J. Van Herle, A.J. McEvoy, J. Phys. Chem. Solids 55 (1994) 339.
[36] R. Jimenez, T. Kloidt, M. Kleitz, J. Electrochem. Soc. 144 (1997) 582.
[37] M. Kleitz, F. Petitbon, Solid State Ionics 92 (1996) 65.
[38] A.M. Svensson, S. Sunde, K. Nisancioglu, J. Electrochem. Soc. 144 (1997) 2719.
[39] A.M. Svensson, S. Sunde, K. Nisancioglu, J. Electrochem. Soc. 145 (1998) 1390.
[40] M. Liu, J. Electrochem. Soc. 145 (1998) 142.
[41] L. Heyne, in: S. Geller (Ed.), Solid State Electrolytes, Springer, Berlin, 1982, pp. 169.
[42] J. Fleig, J. Maier, J. Electroceram. 1 (1997) 73.
[43] J. Fleig, J. Maier, J. Electrochem. Soc. 144 (1997) L302.
[44] M. Mogensen, S. Primdahl, M.J. Jorgensen, C. Bagger, J. Electroceram. 5 (2000) 141.
[45] C.H. Chen, H. Kruidhof, H.J.M. Bouwmeester, A.J. Burggraaf, J. Appl. Electrochem. 27 (1997) 71.
[46] J.E. ten Elshof, M.H.R. Lankhorst, H.J.M. Bouwmeester, Solid State Ionics 99 (1997) 15.
[47] J.A. Lane, S.J. Benson, D. Waller, J.A. Kilner, Solid State Ionics 121 (1999) 201.
[48] R.A. De Souza, J.A. Kilner, Solid State Ionics 106 (1998) 175.
[49] W. Zipprich, S. Waschilewski, F. Rocholl, H.-D. Wiemhöfer, Solid State Ionics 101–103 (1997) 1015.
[50] S. Carter, A. Selcuk, J. Kajda, J.A. Kilner, B.C.H. Steele, Solid State Ionics 53–56 (1992) 597.
[51] B.C.H. Steele, J.-M. Bae, Solid State Ionics 106 (1998) 255.
[52] T. Kawada, K. Masuda, J. Susuki, A. Kaimai, K. Kawamura, Y. Nigara, J. Mizusaki, H. Yugami, H. Arashi, N. Sakai, H. Yokokawa, Solid State Ionics 121 (1999) 271.
[53] J.S. Newman, Electrochemical Systems, 2nd Edition, Prentice-Hall, Englewood Cliffs, NJ, 1991, pp. 454.
[54] H. Uchida, M. Yoshida, M. Watanabe, J. Electrochem. Soc. 146 (1999) 1.